Photochemistry of Adsorbed Nitrate on Aluminum Oxide Particle Surfaces

Gayan Rubasinghege and Vicki H. Grassian*

Department of Chemistry, University of Iowa, Iowa City, Iowa 52246

Received: March 13, 2009; Revised Manuscript Received: May 11, 2009

Nitrogen oxides, including nitrogen dioxide and nitric acid, react with mineral dust particles in the atmosphere to yield adsorbed nitrate. Although nitrate ion is a well-known chromophore in natural waters, little is known about the surface photochemistry of nitrate adsorbed on mineral particles. In this study, nitrate adsorbed on aluminum oxide, a model system for mineral dust aerosol, is irradiated with broadband light ($\lambda > 300$ nm) as a function of relative humidity (RH) in the presence of molecular oxygen. Upon irradiation, the nitrate ion readily undergoes photolysis to yield nitrogen-containing gas-phase products including NO_2, NO, and N_2O, with NO being the major product. The relative ratio and product yields of these gas-phase products change with RH, with N_2O production being highest at the higher relative humidities. Furthermore, an efficient dark reaction readily converts the major NO product into NO_2 during post-irradiation. Photochemical processes on mineral dust aerosol surfaces have the potential to impact the chemical balance of the atmosphere, yet little is known about these processes. In this study, the impact that adsorbed nitrate photochemistry may have on the renoxification of the atmosphere is discussed.

Introduction

In the atmosphere, surface-adsorbed nitrate on particulate matter, for example, mineral dust and sea-salt aerosol, comes from heterogeneous reaction of gas-phase nitrogen oxides including NO_2 and HNO_3 with these particles.[1,2] NO_x ($NO + NO_2$) represents the major gas-phase nitrogen-containing anthropogenic pollutant, produced as a result of automobile and industrial fuel combustion.[3] In the lower atmosphere, these nitrogen oxides participate in a complex series of chemical and photochemical reactions to produce tropospheric ozone in a nonlinear relationship with respect to the ozone concentrations. Therefore, peak ozone levels are affected by the amount of NO_x present in the gas phase, which depends on the ground base emissions and subsequent reactions in the lower atmosphere.[4−6] Moreover, as noted above, atmospheric nitric acid, the main reservoir species in the NO_x cycle,[5] can readily react with particulate matter in the atmosphere to yield adsorbed nitrate.[4] Therefore, understanding all processes that impact NO_x and reservoir species such as HNO_3 is important in atmospheric chemistry and air quality.

Oxide minerals represent an important and reactive component of mineral dust aerosol. Given the fact that aluminum oxides and aluminum silicates contribute ∼8% by mass to the total dust burden in the atmosphere,[7−9] aluminum oxides can be used as model systems to begin to understand various aspects of nitrogen oxide reactions on mineral dust aerosol. Several experimental and theoretical studies have shown that heterogeneous uptake of nitric acid on aluminum oxide and aluminosilicates yields a chemisorbed nitrate layer on the particle surface.[4,7,10−12] Vibrational frequencies of adsorbed nitrate have been assigned and interpreted using quantum chemical calculations of binuclear alumina cluster models.[7] Under humid conditions, atmospheric water vapor readily adsorbs to oxide particles and dissociates, resulting in a hydroxyl-terminated surface.[13] Adsorbed water can hydrogen bond to these hydroxyl groups in equilibrium with water vapor. It has been shown that coadsorbed water molecules readily solvate adsorbed nitrate ions on the aluminum oxide surface forming inner and outer sphere complexes.[7]

Although nitric acid adsorption and water uptake on aluminum oxide surfaces have been previously studied, much less is known about the photochemistry of adsorbed nitrate on these particle surfaces. In natural waters, nitrate is an important chromophore[14,15] with an absorption in the solar region of the spectrum at 302 nm ($\varepsilon = 7.2\ M^{-1}\ cm^{-1}$) attributed to the n-to-π^* electronic transition. Excitation of this transition results in the photochemical production of nitrogen dioxide and nitrite ion under acidic conditions.[16−19] This study is a follow up to a previously published communication[20] that showed that the photochemistry of adsorbed nitrate resulted in the formation of several gas-phase products including N_2O, NO, and NO_2. Besides the important ramifications of this photochemical reaction converting nitrate into NO_x and N_2O, another interesting point of the earlier study is that the product distribution is dependent on the ambient conditions, that is, RH and the presence of molecular oxygen. Here we expand on this initial investigation and more thoroughly investigate the relative humidity (RH) dependence of the reaction products and kinetics. In addition, we present a study of a surface-mediated dark reaction converting NO to NO_2 during post-irradiation.

Experimental Section

Sources of the Oxide Powder and Other Reagents. Commercially available γ-Al_2O_3 (Degussa, aluminum oxide C) with a surface area of $101 \pm 4\ m^2\ g^{-1}$ was used in these experiments. The surface area was determined using a Quantachrome Nova 4200e multipoint BET apparatus. Dry gaseous nitric acid was taken from the vapor of a 1:3 mixture of concentrated HNO_3 (70.6% HNO_3, Mallinckrodt) and 95.9% H_2SO_4, (Mallinckrodt). Distilled H_2O (Fisher, Optima grade) was degassed prior to use.

* To whom correspondence should be addressed. E-mail: vicki-grassian@uiowa.edu.

10.1021/jp902252s CCC: $40.75
Published on Web 06/17/2009

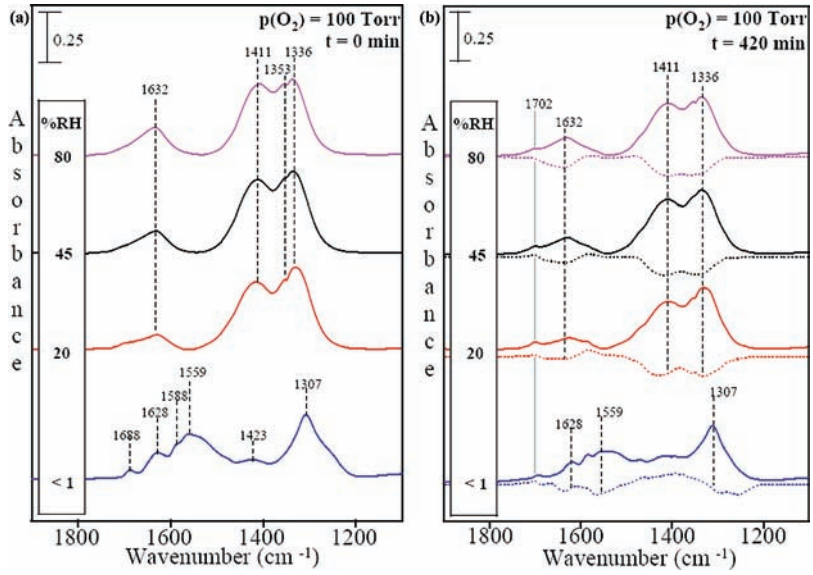

Figure 1. FTIR spectra of surface-adsorbed nitrate under different relative humidity conditions (RH < 1, 20, 45, and 80%) and 298 K (a) before broadband irradiation ($t = 0$ min) and (b) after 420 min of irradiation ($t = 420$ min) (solid line). Each spectrum was referenced to the clean oxide spectrum prior to exposure to nitric acid. Gas-phase absorptions were then subtracted from each spectrum. The dashed-line spectra shown in part b are the difference spectra obtained by subtracting the spectral data at time $t = 420$ min from those at $t = 0$ min. Some of the more notable absorptions that decrease and increase in intensity with irradiation are marked in part b.

Transmission Fourier Transform Infrared Spectroscopy. Photochemistry of adsorbed nitrate was monitored via transmission FTIR spectroscopy. The infrared cell consists of a stainless steel cube with two barium fluoride windows and a sample holder. The inside of the stainless steel cube is coated with Teflon to avoid HNO_3 decomposition on the walls of the infrared cell. For these measurements, the oxide powder (5.7 ± 0.4 mg) was prepared by pressing onto half of a tungsten grid and the other half of the grid was left blank for gas-phase measurements. The oxide samples prepared on the tungsten grid are secured inside the infrared cell by Teflon-coated sample holder jaws. The sample cell is connected to a chamber through a Teflon tube that contains ports for gas introduction and two absolute pressure transducers (range 0.001−10.000 and 0.1−1000.0 Torr). The total volume of the infrared cell is 1214 ± 4 mL (infrared cube 197 ± 2 mL and mixing chamber 1044 ± 1 mL). The vacuum chamber consists of a two-stage pumping system, a turbomolecular/mechanical pump for pumping to 10^{-7} Torr, and a mechanical pump for rough pumping to 10^{-3} Torr. The infrared cell is mounted on a linear translator inside the FT-IR spectrometer. The translator allows both halves of the grid, the blank side for gas-phase measurements and the oxide-coated side for surface measurements, to be probed by simply moving the infrared cell through the IR beam path. After the aluminum oxide surface was exposed to relatively high pressures of nitric acid (1.78 ± 0.01 Torr) for 30 min to saturate the surface with nitrate, the FTIR cell was evacuated overnight to remove all weakly adsorbed products.

Following the introduction of water vapor, molecular O_2 (100 ± 2 Torr), or both, the valve connecting the FTIR cell to the mixing chamber was closed, letting the gas-phase products accumulate inside the cell as the surface was irradiated. In these studies, a 500 W broadband Hg arc lamp (Oriel, model no. 66033), followed by a water filter to remove IR radiation and a filter to remove shorter wavelengths ($\lambda < 300$ nm, Oriel filter no. 59425), was used to irradiate the surface. The intensity of the broadband light source, reaching to the sample inside the custom-made IR cell, was measured using a solar cell (model EI-100, Optical Energy Technologies). Irradiance of the lamp output was measured using a spectroradiometer (model RPS900-R, International Light Technologies). According to these measurements, adsorbed nitrate receives broadband light approximately equal to one solar constant. After irradiation, infrared spectra were recorded with a single-beam Mattson RS-10000 spectrometer equipped with a narrow band MCT detector. Typically, 250 scans were collected with an instrument resolution of 4 cm^{-1} in the spectral range extending from 900 to 4000 cm^{-1}. We obtained absorbance spectra for gas and adsorbed species by referencing single-beam spectra of the blank grid and the oxide-coated grid to single beam spectra collected prior to the nitric acid exposure. To investigate surface-mediated post irradiation processes, the light source was turned off and IR spectra (25 scans, 4 cm^{-1} resolution) were immediately collected of the gas phase every 3 min for 2 h.

Ex Situ X-ray Photoelectron Spectroscopy. The irradiated aluminum oxide sample was removed from the tungsten grid and analyzed using a custom-designed Kratos Axis Ultra X-ray photoelectron spectrometer with a monochromatic Al Kα X-ray source. The sample was pressed onto an indium foil on a copper stub and introduced into the XPS analysis chamber, which had a pressure that was maintained in the 10^{-9} Torr range during analysis. Wide energy range survey scans are acquired using the following parameters: energy range from 1200 to −5 eV, pass energy of 160 eV, step size of 1 eV, dwell time of 200 ms, and X-ray spot size of 700×300 mm^2. High-resolution spectra are acquired using the following parameters: energy range of 50 to 20 eV depending on the peak examined, pass energy of 20 eV, step size of 0.1 eV, and dwell time of 1000 ms. The data collected are analyzed using CasaXPS data processing software. The instrument and data reduction are described in detail in ref 21.

Results and Discussion

Fourier Transform Infrared Spectroscopy of Adsorbed Nitrate before and after Irradiation as *f*(%RH). The transmission FTIR spectra of γ-Al_2O_3 exposed to nitric acid vapor followed by evacuation are shown in Figure 1a at four different

TABLE 1: Percent Nitrate on the Surface Following Broadband Irradiation ($\lambda > 300$ nm) under Different Conditions[a,b]

irradiation time/min	%RH < 1		20 ± 2	45 ± 2		80 ± 2
	with O_2	without O_2	with O_2	with O_2	without O_2	with O_2
30	95 ± 1	83 ± 3 (84 ± 1)[c]	89 ± 1	90 ± 1	72 ± 2 (74 ± 1)[c]	93 ± 1
120	85 ± 1	61 ± 3 (65 ± 2)[c]	78 ± 3	80 ± 2	60 ± 2 (62 ± 1)[c]	82 ± 1
420	82 ± 1	41 ± 8 (44 ± 3)[c]	74 ± 1	77 ± 2	40 ± 3 (43 ± 2)[c]	79 ± 1

[a] At $t = 0$ min, there is 100% nitrate on the surface. [b] Reported nitrate loss is the mean of triplicate measurements, and error represents $\pm 1\sigma$. [c] In select experiments, nitrogen (N_2) was used as a buffer gas at a pressure of 100 Torr, and these data are reported in parentheses. See the text for further details.

relative humidities, <1, 20, 45, and 80%. Under conditions of lowest RH (%RH < 1), adsorbed nitrate binds to the oxide surface in different modes of coordination as monodentate, bidentate, and bridging, as previously discussed in detail, on the basis of the assignment of the peaks in the nitrate ion ν_3 spectral region between 1200 and 1650 cm^{-1}.[4,7] In the presence of water vapor at different relative humidities (20, 45, and 80%), co-adsorbed water solvates the nitrate ion, forming inner and outer sphere complexes that are represented by peaks in the region between 1300 and 1450 cm^{-1} in Figure 1a.[7] Changes in the infrared spectra as a function of RH and the assignment of these peaks have been discussed extensively, and the details can be found in refs 4 and 7.

Following the adsorption of nitric acid and the introduction of water vapor adjusted to the different relative humidities, the sample was irradiated with the broadband light ($\lambda > 300$ nm). Upon irradiation, the FTIR spectra of the nitrated surface at each RH were recorded. It can be seen in Figure 1b that the spectrum changes after 420 min of irradiation. Most notably, there is a decrease in the intensity of the spectral bands associated with adsorbed nitrate. An analysis of the changes in the intensities of these bands, including an analysis of the difference spectra, shows that there is a loss of intensity at low RH near 1559 cm^{-1}, assigned to the monodentate adsorbed nitrate, and the bands at 1588 and 1307 cm^{-1}, assigned to bridging nitrate. That is to say that the monodentate species shows the greatest loss upon irradiation, followed by bridging nitrate absorptions. This reveals that there is a greater propensity for certain oxide-coordinated adsorbed nitrates to undergo photolysis. At higher RH, the solvated nitrate peaks, observed between 1300 and 1450 cm^{-1}, all decrease upon irradiation.

The percent loss of surface nitrate as a function of irradiation time is given in Table 1. The percent loss is determined using normalized integrated absorbance of the entire adsorbed nitrate ν_3 region extending from ca. 1220 to 1700 cm^{-1} for %RH < 1 and from 1200 to 1550 cm^{-1} for solvated nitrate at higher RH. The effect of molecular oxygen on nitrate photolysis was studied under two different RH conditions: %RH < 1 and %RH 45 ± 2. In both the cases, the surface nitrate loss decreased significantly in the presence of molecular oxygen. As shown in Table 1, under dry conditions, the total nitrate on the surface decreases from 100% (at time $t = 0$) to 82 ± 1 and 41 ± 8% in the presence and absence of molecular oxygen, respectively, following 420 min of irradiation. Similar changes are observed under humid conditions, 77 ± 2 and 40 ± 3%, upon irradiation in the presence and absence of molecular oxygen, respectively. Control experiments in the presence of molecular nitrogen reveal that changes in the amount of surface nitrate loss are a result of interaction of the surface with molecular oxygen and not just due to the presence of a buffer gas. In a number of experimental and theoretical studies, it has been reported that defect sites including the presence of neutral oxygen vacancies and charged oxygen vacancies are present on aluminum oxide.[22] These

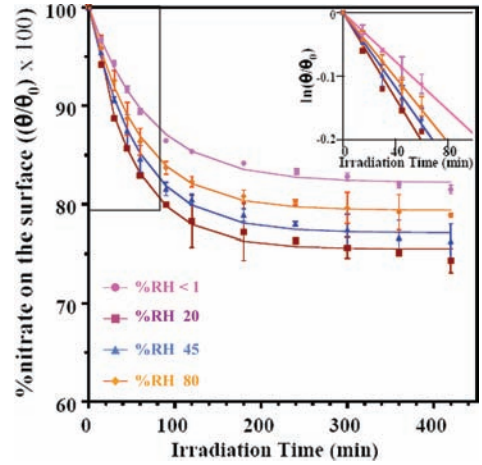

Figure 2. Photo-induced surface nitrate loss in the presence of molecular oxygen under different relative humidity conditions (RH < 1, 20, 45, and 80%). θ_o-adsorbed nitrate concentration on saturated oxide surface at $t = 0$. θ-nitrate concentration on oxide surface at irradiation time, t. The presented nitrate loss is the mean of triplicate measurements, and the error bars represent the standard deviation.

O(vacancy) sites may play a role, albeit unknown, in the primary photochemical process of adsorbed nitrate or the chemistry of photoproducts. If these sites are primary binding sites for the adsorption of molecular oxygen, then oxygen will have a large impact on the photochemistry of adsorbed nitrate, as is evident in these studies.

As seen in Table 1, the effect of RH on adsorbed nitrate photolysis is more significant in the presence of molecular oxygen. In the oxidative environment provided by the presence of molecular oxygen, a higher nitrate loss was recorded under humid conditions compared with that of dry (%RH < 1). To understand the effect of RH on nitrate photolysis further, more experiments were carried out under additional conditions of RH in the presence of molecular oxygen. The higher loss of surface nitrate under humid conditions can be attributed to the formation of inner and outer sphere complexes of nitrate ion, which have less interaction with the surface and less molecular distortion from the planar D_{3h} symmetry of the free ion compared with the oxide coordinated nitrate structures present under dry conditions.[7] Furthermore, in the presence of water vapor, there is a possibility of forming hydroxyl radicals as a result of nitrate photolysis.[14,23] These hydroxyl radicals can initiate new photochemical pathways leading to a higher nitrate loss from the oxide surface.[24] H-bonding between solvated nitrate and coadsorbed water affects the energetics of the electronic n-to-π^* transition near 300 nm with a red shift resulting in a higher overlap of the absorption profile of nitrate with the broadband irradiation source.[13,25]

According to Figure 2, during several hours of photolysis of adsorbed nitrate, the change in the rate of nitrate disappearance is most significant in the first 90 min. An attempt to fit the time dependence of nitrate photolysis to first-order kinetics to gain

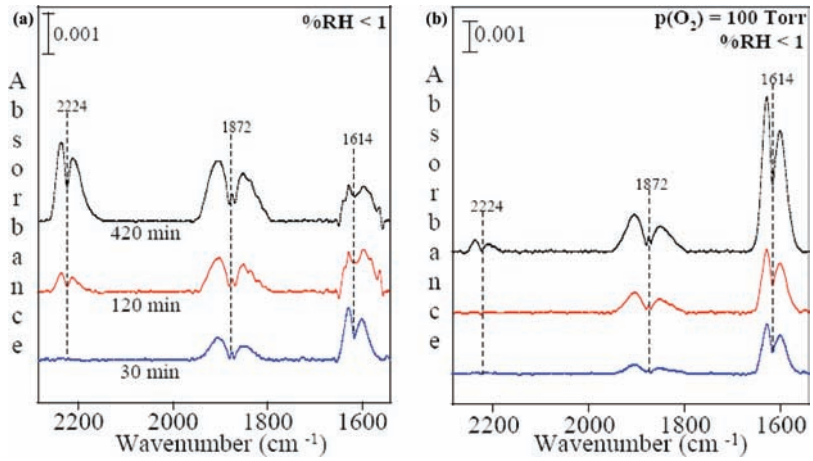

Figure 3. FTIR spectra of gas-phase products formed during photolysis of adsorbed nitrate under dry conditions (%RH < 1) at 298 K (a) in the absence of molecular oxygen and (b) in the presence of molecular oxygen (100 ± 5 Torr). Each spectrum was referenced to the gas-phase spectrum prior to exposure to nitric acid.

an estimate of an apparent rate constant is shown in the inset of Figure 2. According to this analysis, the first-order photolysis rate constants are $(3.2 \pm 0.2) \times 10^{-5}$, $(5.6 \pm 0.3) \times 10^{-5}$, $(4.9 \pm 0.2) \times 10^{-5}$, and $(4.2 \pm 0.2) \times 10^{-5}$ s^{-1} for RH < 1, 20, 45, and 80%, respectively. Therefore, the initial rate of adsorbed nitrate photolysis is approximately 1.5 to 2 times faster in the presence of co-adsorbed water.

Along with the photochemical loss of nitrate, there is the growth of product bands as well. As seen in the spectra shown in Figure 1b, there is a peak near 1702 cm^{-1} that grows in intensity, under all conditions of RH. The presence of the band at 1702 cm^{-1} on the surface suggests the formation of a new surface product. The assignment of this band as well as the assignment of several nitrogen-containing gas-phase products are discussed in detail below.

Analysis of Gas-Phase and Surface-Bound Products. As shown in Figure 3, gas-phase products appear as a function of irradiation of adsorbed nitrate. FTIR spectra of these gas-phase products recorded as a function of irradiation time under dry conditions (%RH < 1) in both the presence and absence of molecular oxygen are shown. It is relatively easy to identify the major gas-phase products to be N_2O, NO, and NO_2 with characteristic absorptions at 2224, 1872, and 1614 cm^{-1}, respectively.[20] A comparison of the spectra shown in Figure 3a, b reveals a significant change in the gas-phase product distribution, in particular the relative N_2O and NO_2 concentrations under these two different environmental conditions. This large difference was noted and previously discussed in our earlier study.[20] Therefore, in this work we focus more on gas product distribution under different RH conditions in an oxidative environment, that is, in the presence of molecular oxygen, because this is more atmospherically relevant conditions.

Gas-phase concentrations obtained from FTIR analysis, followed by broadband ($\lambda > 300$ nm) irradiation of adsorbed nitrate in the presence of molecular oxygen under the different RH conditions (RH < 1, 20, 45, and 80%) are shown in Figure 4. The results presented in Figure 4 are the average value of triplicate measurements, and the reported error represents one standard deviation. We determined gas-phase concentrations of individual species by converting integrated absorbances to concentrations using calibration factors for the individual gas-phase species. These data show that gas-phase NO_2, NO, and N_2O are produced at different rates and in different yields.

Before further discussing the photochemistry of adsorbed nitrate and the photoproducts that form, it is first instructive to consider what is known about nitrate photochemistry in solution phase and snowpack. It is well known that irradiation of the nitrate ion with light at 305 nm under acidic conditions yields nitrogen dioxide and nitrite. Further photolysis of the nitrite ion at 365 nm produces NO,[14,16−19] according to the following reactions

$$NO_3^- + H^+ \xrightarrow{305\ nm} NO_2 + OH \quad (1)$$

$$NO_3^- \xrightarrow{305\ nm} NO_2^- + O(^3P) \quad (2)$$

and

$$NO_2^- + H^+ \xrightarrow{365\ nm} NO + OH \quad (3)$$

The current results for the surface photochemistry of adsorbed nitrate can begin to be explained in the framework of nitrate ion photochemistry in acidic aqueous media, as shown by reactions 1−3. Figure 4 shows that during the first 30 min of irradiation, adsorbed nitrate yields NO_2 as the major gas-phase product in the presence of co-adsorbed water. However, for longer irradiation times, that is, after 120 and 420 min, the major gas-phase product is seen to be NO, followed by NO_2 and N_2O. This change in gas-phase product distribution may partially be associated with gas-phase NO_2 photochemistry to yield NO. In a reaction cell with only gas-phase NO_2 present, photolysis is measured and determined to be 200-fold faster compared with adsorbed nitrate photolysis.

In addition, N_2O production is higher under the highest RH conditions. These variations in the gas-phase product distribution can be seen more clearly in the plots shown in Figure 5. These plots, showing the relative gas-phase concentrations of NO_2, N_2O, and NO at short (30 min), medium (120 min), and longer (420 min) irradiation times, were obtained by normalizing the gas-phase concentrations to the largest gas-phase product species in a given RH, which is NO at long times in all cases.

As can be seen in the data shown in Figures 4 and 5, the gas-phase NO_2 concentration increases to %RH 20 and slightly decreases after %RH 45. Under higher RH conditions, that is,

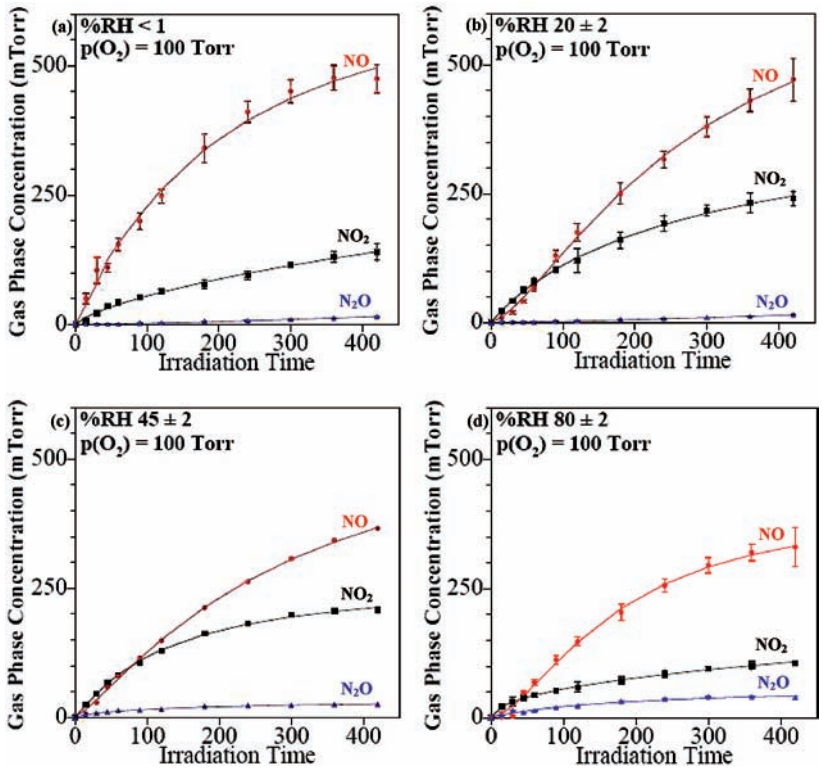

Figure 4. Gas-phase concentrations obtained from FTIR spectra following irradiation of adsorbed nitrate in the presence of molecular oxygen at 298 K under different relative humidity (%RH) conditions: (a) <1, (b) 20 ± 2, (c) 45 ± 2, and (d) 80 ± 2.

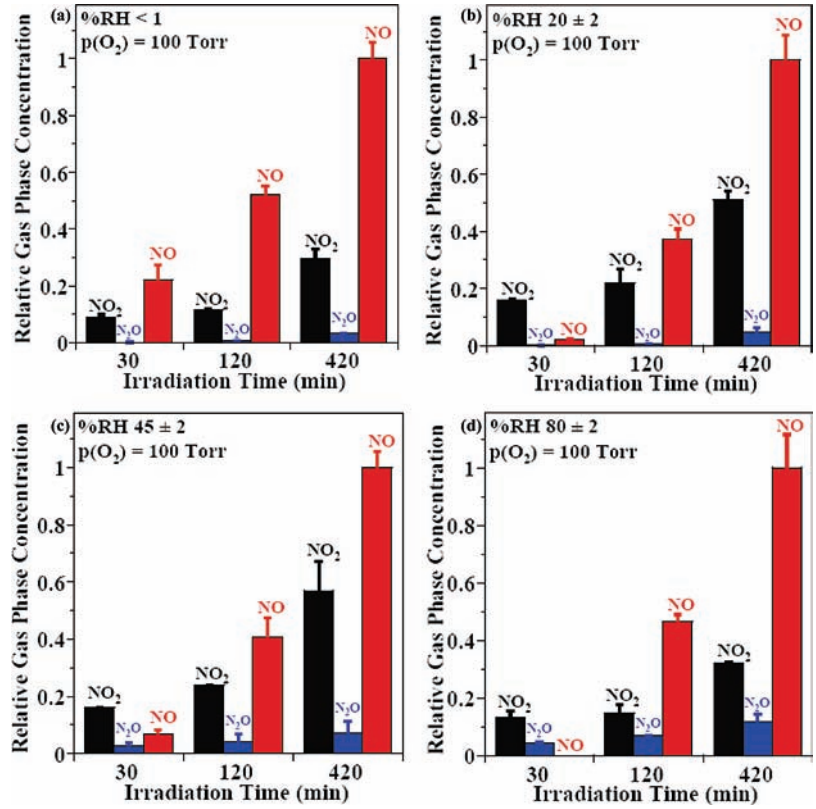

Figure 5. Relative gas-phase concentrations obtained from FTIR spectra following irradiation of adsorbed nitrate in the presence of molecular oxygen at 298 K under different relative humidity (%RH) conditions: (a) <1, (b) 20 ± 2, (c) 45 ± 2, and (d) 80 ± 2 at short (30 min), medium (120 min), and longer (420 min) irradiation times. The gas-phase concentrations have been normalized to the largest gas-phase product species after 420 min of irradiation.

%RH 45 and 80, there is a possibility to react NO_2 with co-adsorbed water to yield solvated nitrate on the surface.[26,27] The readsorption of gas-phase products is discussed in detail in the discussion of post-photolysis processes. Photolysis of NO_2^- to NO is not predominant under humid conditions during the first 30 min of irradiation. Formation of $[NO_2^- \cdot H_2O]$ in the presence

of co-adsorbed water and lower acidity may be the possible reasons for the above observation. In addition, protons (H^+) generated from adsorbed water are utilized in a competitive reaction during the formation of N_2O under these conditions, as discussed below. Furthermore, as irradiation proceeds, the accumulation of nitrite may favor the production of NO. Although attempts to detect surface-adsorbed nitrite were unsuccessful, it potentially may be present at very low level steady-state coverages under these conditions.

As we previously reported, the formation of nitrous oxide (N_2O) is observed during the photolysis of adsorbed nitrate. The relative N_2O concentration is highly significant in the absence of molecular oxygen and also contributes to a major fraction in the presence of oxygen under humid conditions at the end of 7 h of photolysis. As we have previously discussed, surface-catalyzed reactions of NO can lead to the formation of N_2O, which is easily quenched in the presence of molecular oxygen.[28] Malecki and Malecka, in their studies on thermal decomposition of metal nitrates, have proposed two other possible reaction mechanisms for the formation of N_2O in the presence of NO and NO_2.[29]

$$\text{Mechanism 1} \quad NO_2 + NO_3^- \rightarrow N_2O + 7/4\ O_2 + 1/2\ O_2^- \tag{4}$$

$$\text{Mechanism 2} \quad 2NO \rightarrow N_2O_2 \tag{5}$$

$$N_2O_2 + NO \rightarrow N_2O + NO_2 \tag{6}$$

In the presence of oxygen, N_2O_2 can be oxidized to yield NO_2

$$N_2O_2 + O_2 \rightarrow 2NO_2 \tag{7}$$

In addition, Maric et al. also have shown a similar mechanism for the formation of N_2O via a heterogeneous dark conversion of NO_2, N_2O_5, or both.[30] The above two pathways provide possible mechanisms for the production of N_2O and changes in the relative gas-phase concentrations of N_2O and NO_2, respectively, in the presence of molecular oxygen under dry conditions. At higher relative humidities, particularly at %RH 45 and 80, a significant amount of gas-phase N_2O was observed, even in an oxidizing environment. In previous studies on heterogeneous hydrolysis of NO_2, it has been shown that N_2O is produced under humid conditions and longer reaction times.[27] Recently, Wiesen et al. and Kleffmann et al. have described a possible reaction mechanism for the formation of N_2O via HONO in their studies on the hydrolysis of NO_2 on an acidic surface.[31−33] The overall reaction of the proposed mechanism has been described as

$$8NO_2 + 3H_2O \xrightarrow{[H^+]} N_2O + 6HNO_3 \tag{8}$$

In this reaction pathway, the hyponitrous acid (HON═NOH) intermediate is proposed to decompose to N_2O over a wide pH range, including acidic conditions.[34−36] These mechanisms and the pathways discussed for NO_2 surface reactions under humid conditions suggest that the higher relative gas-phase concentration of N_2O is due to a secondary reaction of NO_2 on the acidic oxide surface. This can also be one of the potential reasons for the observed lower gas-phase NO_2 concentrations under extreme RH conditions at which the N_2O production is highest. The formation of HONO and its photochemical products are further discussed below.

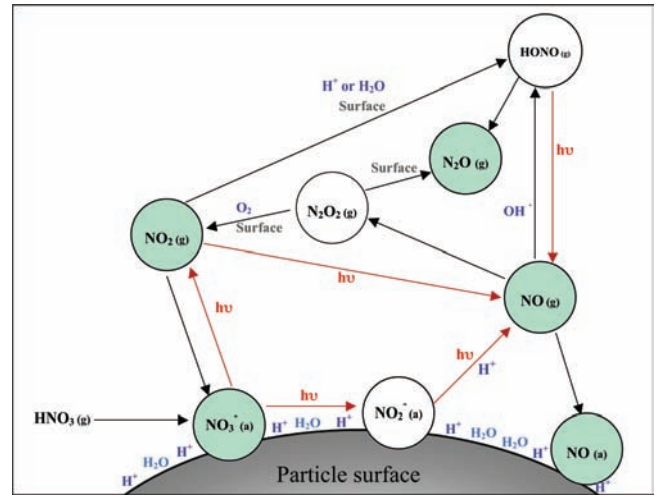

Figure 6. Schematic of the reaction mechanism of heterogeneous photolysis of adsorbed nitrate. HNO_3(g) (left side of the diagram) adsorbs from the gas phase onto the surface to yield nitrate ion (NO_3^-(a)) and protons (H^+) in the presence and absence of coadsorbed water. Broadband irradiation results in the production of gas-phase and surface-adsorbed products, as shown by the different species. The observed gas-phase and surface-bound products in the transmittance FTIR spectroscopy are colored green, whereas gas-phase and surface-bound proposed intermediates not detected by FTIR spectroscopy including gas-phase N_2O_2 and HONO and adsorbed NO_2^- are shown in white.

Because NO is the major gas-phase product, there is a possibility of readsorbing NO on the aluminum oxide surface. In previous studies, vibrational modes of adsorbed NO have been reported and assigned to bands at ~1700−1720 cm^{-1} on different surfaces.[37−40] The adsorption band near 1702 cm^{-1} in the adsorbed phase spectra that grows during irradiation is most likely due to NO adsorbed to oxide surfaces. Furthermore, the X-ray photoelectron spectrum (XPS) in the N(1s) region of the irradiated nitrated aluminum oxide surface revealed a peak at 401 eV, which was not observed in the XPS of samples exposed to nitric acid and not irradiated. The peak at 401 eV is consistent with the presence of adsorbed NO on the surface.[41] For both samples that were just exposed to nitric acid and those exposed to nitric acid and irradiated, a peak at 407 eV was present in the N(1s) region. This higher energy peak is consistent with adsorbed nitrate on the surface. Higher production of NO_2 in the presence of O_2 can lead to NO_2 adsorption on the surface to yield adsorbed nitrates, thus contributing as another source to the overall nitrate on the surface.

In recent studies, evidence of photochemical generation of nitrous acid, HONO, from the surface reaction of hydroxyl radicals with nitrogen dioxide in the presence of water vapor is available.[42−46] Furthermore, it is reported that HONO flux is wavelength dependent, and its release is strongest when $\lambda <$ 320 nm, where the absorption of aqueous nitrate is highest.[47] Again, gas-phase HONO can be photochemically converted back to NO and OH.[42] In these studies HONO was not observed in the gas phase, although its photolysis product NO is readily observed.

The schematic of the proposed reaction mechanism of heterogeneous photolysis of adsorbed nitrate is shown in Figure 6. Heterogeneous uptake of nitric acid, HNO_3(g), on the left side of the diagram yields nitrate ion (NO_3^-(a)) and protons

(H^+) on the surface in the presence and absence of coadsorbed water. Upon broadband irradiation, NO and NO_2 are produced as major gas-phase products. Photochemistry of gas-phase NO_2 yields NO, which makes NO the dominant product. In the absence of O_2, NO acts as the precursor for N_2O via a surface-mediated reaction, whereas the reaction mechanism is poisoned in the presence of molecular oxygen, resulting in more NO_2 and less N_2O. In the presence of coadsorbed water, NO_2 becomes the precursor for gas-phase N_2O through heterogeneous hydrolysis of NO_2 on the acidic surface. The proposed mechanism involves gas-phase species of N_2O_2 and HONO, whereas NO_2^-(a) is an intermediate of gas-phase NO formation via photolysis. In addition, the gas-phase species are readsorbed onto the surface as nitrate and NO(a).

Dark Reaction: Gas-Phase Product Distribution Changes Postphotolysis Involving a Surface-Catalyzed Reaction. Relative gas-phase distributions presented in the last section for %RH < 1 and %RH 45 differ from that reported in our previous work. In the earlier work, following photolysis, the lamp was turned off and the FTIR sample compartment was purged for several minutes prior to recording a spectrum so as to remove CO_2 and H_2O from the FTIR compartment with dry air. In the current study, the apparatus was modified so that the lamp was incorporated into the dry air purge box so that extra purge time post-photolysis was unnecessary in these current experiments. During the time it took to purge the compartment, there were changes in the gas-phase product distribution, unbeknownst in the earlier studies. This change in the gas-phase distribution observed here led us to investigate this postphotolysis dark reaction further.

FTIR spectra collected every 3 min of the gas phase immediately after the broadband light source was turned off are shown in Figure 7a. As seen in the spectra, the N_2O concentration remains constant with time, whereas the NO concentration decreases concomitant with an increase in the NO_2 concentration. As shown in Figure 5b, at RH < 1%, the NO_2 concentration reaches a maximum after around 100 min, and NO decays during this period. The same effect was observed under all humidity conditions investigated. However, at higher RH, NO_2 reached a maximum in a shorter time period. The basic chemical reaction most likely responsible for this gas-phase conversion is

$$2NO + O_2 \rightarrow 2NO_2 \qquad (8a)$$

The oxidation of NO to NO_2 is an important intermediate step involved in NO_x abatement that is being developed for diesel engines.[48] It is also the first step that occurs in the cyclic NO_x storage and recycle process.[49]

Relative gas-phase distributions after 120 min of post-photolysis under different experimental conditions are shown in Figure 5c. In contrast with the distributions given in Figure 5, NO_2 is the dominant product in the dark under the most atmospherically relevant conditions, that is, under humid conditions and in the presence of molecular oxygen. The relative gas-phase concentration of N_2O appears to be increasing under humid conditions.

Conclusions and Atmospheric Implications

The photochemical conversion of nitric acid to gas-phase nitrous oxide, nitric oxide, and nitrogen dioxide through an adsorbed nitrate intermediate under different atmospherically relevant conditions has been shown. Under humid conditions,

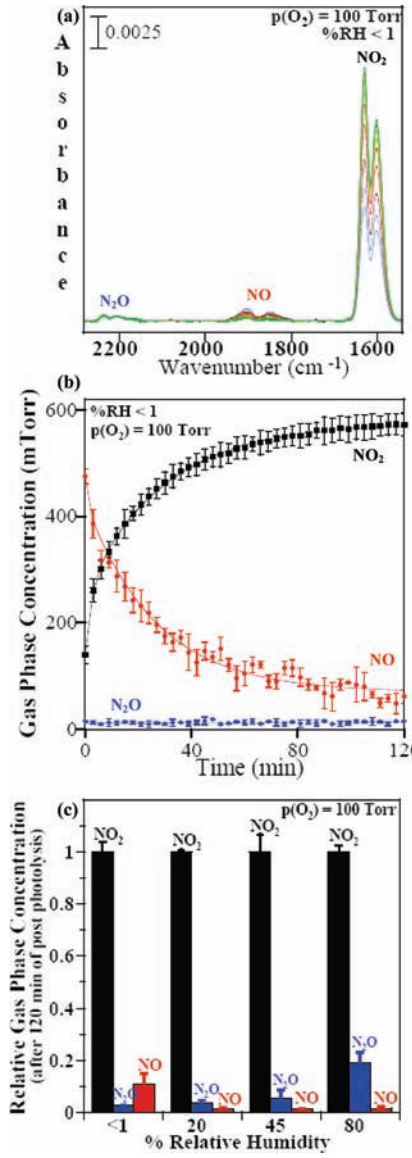

Figure 7. Changes in the gas-phase product distribution during post-irradiation of adsorbed nitrate. (a) FTIR spectra of gas-phase products collected under %RH < 1 following irradiation for 420 min. (b) Change of gas-phase product (NO and NO_2) concentrations as a function of time under %RH < 1 following irradiation. (c) Relative gas-phase concentrations after 120 min of post-photolysis under different RH conditions.

photolysis of solvated nitrate is higher than that of oxide-coordinated nitrate under dry conditions. This could be a potentially important, yet previously unknown, surface-mediated photochemical pathway in the NO_y cycle. Here we reported the production of N_2O, an important greenhouse gas, with higher concentrations under humid conditions in the presence of molecular oxygen. We propose that this reaction involves a heterogeneous conversion of gas-phase NO and NO_2. Higher relative gas-phase concentrations of N_2O under humid conditions can be attributed to a secondary reaction of NO_2 on acidic oxide surfaces. The present work also focused on the chemistry of surface-mediated gas-phase product distribution changes. In the dark, gas-phase NO is oxidized to NO_2 in the presence of O_2, whereas the N_2O concentration remains constant. The rate of this gas-phase conversion increases as a function of RH because of increased readsorption of NO_2 back to the surface under humid conditions. The higher oxidation rates of NO by molecular oxygen suggest an involvement of the oxide surface

in the reaction mechanism. Therefore, we propose a surface-mediated dark reaction for the above gas-phase conversion.

These results have implications for atmospheric processes involving nitric acid, NO_x, and mineral dust aerosol. Furthermore, the results provide some evidence of photochemical reactions of atmospheric significance taking place on the surface of particulate matter. This study also reveals that in the troposphere, NO_x level can be affected by these continued reactions of adsorbed nitrate initiated by sunlight. Moreover, the heterogeneous photochemical conversion of nitric acid to NO_x could contribute to renoxification of the atmosphere. In atmospheric field studies, the interpretation of observed trends in terms of reaction mechanisms is difficult because of the involvement of a complex blend of substrates distributed in several phases and the lack of knowledge in composition of particulate matter such as mineral dust and sea salt and their behavior under different atmospheric conditions. Therefore, detailed studies, such as this one of potential reactions involving heterogeneous photochemistry of associated secondary species such as nitrate on aerosols, may be useful in better explaining field results of atmospheric chemistry and may be implemented in atmospheric chemistry models that can be used to explain and predict concentrations of key gas-phase constituents under a variety of environmental conditions.

Acknowledgment. This material is based on the work supported by the National Science Foundation under grant CHE0503854. Any opinions, findings, and conclusions or recommendations expressed in this material are those of authors and do not necessarily reflect the views of the National Science Foundation.

References and Notes

(1) Usher, C. R.; Michel, A. E.; Grassian, V. H. *Chem. Rev.* **2003**, *103*, 4883.
(2) Laskin, A.; Iedema, M. J.; Cowin, J. P. *Environ. Sci. Technol.* **2002**, *36*, 4948.
(3) Kato, N.; Akimoto, H. *Atmos. Environ., Part A* **1993**, *27*, 1163.
(4) Goodman, A. L.; Bernard, E. T.; Grassian, V. H. *J. Phys. Chem. A* **2001**, *105*, 6443.
(5) Seinfeld, J. H., Pandis, S. N. *Atmospheric Chemistry and Physics From Air Pollution to Climatic Change*, 2nd ed.; John Wiley and Sons: New York, 2006.
(6) Sillman, S.; Logan, J. A.; Wofsy, S. C. *J. Geophys. Res., [Atmos.]* **1990**, *95*, 1837.
(7) Baltrusaitis, J.; Schuttlefield, J.; Jensen, J. H.; Grassian, V. H. *Phys. Chem. Chem. Phys.* **2007**, *9*, 4970.
(8) Gomes, L.; Gillette, D. A. *Atmos. Environ., Part A* **1993**, *27*, 2539.
(9) Warneck, P. *Chemistry of the Natural Atmosphere*; Academic Press: San Diego, CA, 1988; Vol. 41.
(10) Angelini, M. M.; Garrard, R. J.; Rosen, S. J.; Hinrichs, R. Z. *J. Phys. Chem. A* **2007**, *111*, 3326.
(11) Mashburn, C. D.; Frinak, E. K.; Tolbert, M. A. *J. Geophys. Res., [Atmos.]* **2006**, *111*, D15213.
(12) Hatch, C. D.; Gough, R. V.; Toon, O. B.; Tolbert, M. A. *J. Phys. Chem. B* **2008**, *112*, 612.
(13) Cwiertny, D. M.; Young, M. A.; Grassian, V. H. *Annu. Rev. Phys. Chem.* **2008**, *59*, 27.
(14) Goldstein, S.; Rabani, J. *J. Am. Chem. Soc.* **2007**, *129*, 10597.
(15) Young, M. A. Environmental Photochemistry in Surface Waters. In *Water Encyclopedia*; John Wiley & Sons: New York, 2005.
(16) Boxe, C. S.; Colussi, A. J.; Hoffmann, M. R.; Perez, I. M.; Murphy, J. G.; Cohen, R. C. *J. Phys. Chem. A* **2006**, *110*, 3578.
(17) Chu, L.; Anastasio, C. *J. Phys. Chem. A* **2003**, *107*, 9594.
(18) Mack, J.; Bolton, J. R. *J. Photochem. Photobiol., A* **1999**, *128*, 1.
(19) Zellner, R.; Exner, M.; Herrmann, H. *J. Atmos. Chem.* **1990**, *10*, 411.
(20) Schuttlefield, J.; Rubasinghege, G.; El-Maazawi, M.; Bone, J.; Grassian, V. H. *J. Am. Chem. Soc.* **2008**, *130*, 12210.
(21) Balrusaitis, J.; Usher, C. R.; Grassian, V. H. *Phys. Chem. Chem. Phys.* **2007**, *9*, 3011.
(22) Evarestor, R. A. *Quantum Chemistry of Solids: The LCAO First Principles Treatment of Crystals*; Springer: New York, 2007.
(23) Vione, D.; Maurino, V.; Minero, C.; Pelizzetti, E.; Harrison, M. A. J.; Olariu, R. I.; Arsene, C. *Chem. Soc. Rev.* **2006**, *35*, 441.
(24) González, M. C.; Román, E. S. Environmental Photochemistry in Heterogeneous Media. In *Environmental Photochemistry, Part II*; Springer: Berlin, 2005; Vol. 2, p 49.
(25) Miller, T. M.; Grassian, V. H. *Geophys. Res. Lett.* **1998**, *25*, 3835.
(26) Cheung, J. L.; Li, Y. Q.; Boniface, J.; Shi, Q.; Davidovits, P.; Worsnop, D. R.; Jayne, J. T.; Kolb, C. E. *J. Phys. Chem. A* **2000**, *104*, 2655.
(27) Finlayson-Pitts, B. J.; Wingen, L. M.; Sumner, A. L.; Syomin, D.; Ramazan, K. A. *Phys. Chem. Chem. Phys.* **2003**, *5*, 223.
(28) Trogler, W. C. *Coord. Chem. Rev.* **1999**, *187*, 303.
(29) Malecki, A.; Malecka, B. *Thermochim. Acta* **2006**, *446*, 113.
(30) Maric, D.; Burrows, J. P.; Moortgat, G. K. *J. Atmos. Chem.* **1992**, *15*, 157.
(31) Wiesen, P.; Kleffmann, J.; Kurtenbach, R.; Becker, K. H. *Faraday Discuss.* **1995**, *100*, 121.
(32) Kleffmann, J.; Becker, K. H.; Wiesen, P. *Atmos. Environ.* **1998**, *32*, 2721.
(33) Kleffmann, J.; Becker, K. H.; Wiesen, P. *J. Chem. Soc., Faraday Trans.* **1998**, *94*, 3289.
(34) Hughes, M. N.; Stedman, G. *J. Chem. Soc.* **1964**, 163.
(35) Akhtar, M. J.; Balschi, J. A.; Bonner, F. T. *Inorg. Chem.* **1982**, *21*, 2216.
(36) Loechler, E. L.; Schneider, A. M.; Schwartz, D. B.; Hollocher, T. C. *J. Am. Chem. Soc.* **1987**, *109*, 3076.
(37) Berlier, G.; Spoto, G.; Ricchiardi, G.; Bordiga, S.; Lamberti, C.; Zecchina, A. *J. Mol. Catal A: Chem.* **2002**, *182*, 359.
(38) Kazusaka, A.; Suzuki, H.; Toyoshima, I. *Chem. Commun.* **1983**, 150.
(39) Hu, Y.; Griffiths, K. *Surf. Sci.* **2008**, *602*, 2949.
(40) Hu, Y. H.; Griffiths, K. *Appl. Surf. Sci.* **2008**, *254*, 1666.
(41) Overbury, S. H.; Mullins, D. R.; Huntley, D. R.; Kundakovic, L. *J. Catal.* **1999**, *186*, 296.
(42) Ramazan, K. A.; Syomin, D.; Finlayson-Pitts, B. J. *Phys. Chem. Chem. Phys.* **2004**, *6*, 3836.
(43) Ndour, M.; D'Anna, B.; George, C.; Ka, O.; Balkanski, Y.; Kleffmann, J.; Stemmler, K.; Ammann, M. *Geophys. Res. Lett.* **2008**, *35*, L05812.
(44) Gustafsson, R. J.; Orlov, A.; Griffiths, P. T.; Cox, R. A.; Lambert, R. M. *Chem. Commun.* **2006**, 3936.
(45) Stemmler, K.; Ammann, M.; Donders, C.; Kleffmann, J.; George, C. *Nature* **2006**, *440*, 195.
(46) George, C.; Strekowski, R. S.; Kleffmann, J.; Stemmler, K.; Ammann, M. *Faraday Discuss.* **2005**, *130*, 195.
(47) Bartels-Rausch, T.; Donaldson, D. J. *Atmos. Chem. Phys. Discuss.* **2006**, *6*, 10713.
(48) Xue, E.; Seshan, K.; Vanommen, J. G.; Ross, J. R. H. *Appl. Catal., B* **1993**, *2*, 183.
(49) Castoldi, L.; Matarrese, R.; Lietti, L.; Forzatti, P. *Appl. Catal., B* **2006**, *64*, 25.

JP902252S